Proceedings of the
Annual Stability Conference
Structural Stability Research Council
Louisville, Kentucky, April 13-16, 2021

Experimental verification of eccentrically loaded steel joists with non-symmetric sections

Edward J. Sippel[1], Ronald D. Ziemian[2], Hannah B. Blum[3]

Abstract

Open web steel joists are an economical framing system. Joists are efficiently designed structures that are optimized to carry the intended design loads. A joist requires careful consideration when point loads are added after the original design as it may alter the expected behavior. Current requirements state that additional loading should be applied concentrically; however, this does not always happen. Some common attachments for hanging loads are designed to be connected to a single member of the bottom chord which introduces torsion within the system. Recent work with MASTAN2 has shown the ability to accurately model the response of individual non-symmetric members like those used in the chords and webs in many steel joists. This project sought to verify the ability of MASTAN2 to capture the system response of a steel joist subjected to eccentric loading. An experimental evaluation of a steel joist subjected to uniform loading on the top chord and an eccentric hanging load on one bottom chord angle was performed. Comparisons between the experimental and computational results indicated that MASTAN2 can provide an acceptable prediction of the behavior in a steel joist structure subjected to eccentric loads.

1. Introduction

Open web steel joists are an economical steel framing option with multiple benefits including efficient material usage, ease of erection, and flexibility in design (Murphy, 1992). Steel joists are commonly constructed from open cross sections with chords composed of double angles and webs composed of channels, single angles, or double angles. Steel joists are designed for a specific set of loading conditions which is often a uniformly distributed load assumed to be applied to the top chord. The addition of point loads to the joist takes careful consideration to ensure that there is no overstressing of the joist components, particularly the chords from additional bending effects. As general guidance, the Steel Joist Institute provided the recommendation that point loads which do not exceed 100 pounds and are concentrically loaded as shown in Fig. 1(a) on the chord can likely be supported along the joist without modifications provided the total bending moment and shear forces including the point load are less than the design uniform loading (SJI,

[1]Graduate Research Assistant, University of Wisconsin-Madison, <esippel@wisc.edu>
[2]Professor, Bucknell University, <ziemian@bucknell.edu>
[3]Assistant Professor and Alain H. Peyrot Fellow, University of Wisconsin-Madison, <hannah.blum@wisc.edu>

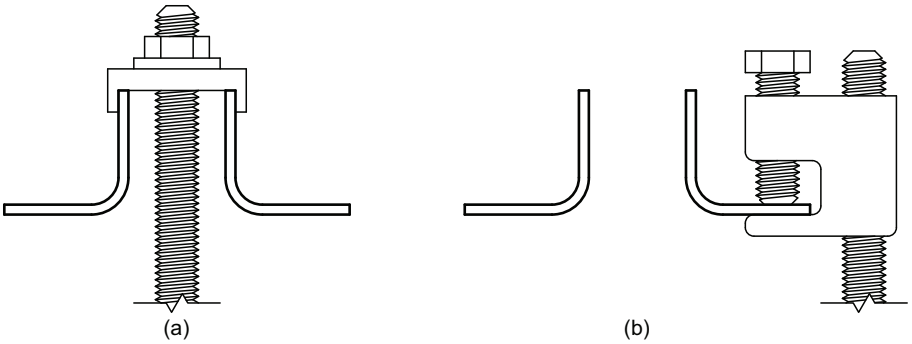

Figure 1: Point load applied to bottom chord using a: (a) concentric connection (b) eccentric connection

2020). If the point load exceeds 100 pounds, it is recommended to add a strut to reinforce the joist and reduce bending. In either case, it is not recommended to load a chord eccentrically as shown in Fig. 1(b) as it introduces torsion that was not previously included in design. Despite not being recommended, many hangers are available on the market and are currently used to support hanging loads from only one of the angle chords. The proper evaluation of the joist in this condition requires additional calculations accounting for eccentricity and bending to approximate the overall response in the chord that are not included in typical joist design.

This evaluation requires the consideration of the non-symmetric behavior of the single angle chord members as well as the overall joist response. Typical structural analysis software with beam (line) elements can be used to assist in determining the overall joist response in accordance with SJI recommendations (Fisher and Green, 2007), but the analysis will only account for the doubly symmetric behavior of the system. Most structural analysis methods would require external consideration of the effects of the non-symmetric properties of the single angle. Liu et al. (2018; 2019) described a new beam element that could be used to include non-symmetric effects in the structural analysis. This element has been included in recent updates to MASTAN2 (Ziemian, McGuire, and Liu, 2019). Numerical verification has shown that MASTAN2 is capable of accurately producing solutions that agree with theoretical results as well as other computational methods (Liu, Ziemian, et al., 2018; Liu, Gao, and Ziemian, 2019; Sippel, Ziemian, and Blum, 2020; Sippel and Blum, 2020). This project sought to verify the results of MASTAN2 with an experimental result. An open web steel joist system was loaded with differing magnitudes of uniform load and then subjected to an eccentric hanging loading on one of the bottom chord angle members. The results from the experimental set-up and the computational models were used to compare the stress distribution calculated in the bottom chord members and displacements.

2. Overview

With the various additions to MASTAN2, the user is capable of analyzing a wide variety of situations and complex systems. While one would be able to model the entire floor system with bracing, in practice an engineer would likely focus their evaluation to a single joist. As this project was concerned with the practical application of MASTAN2, a single joist model was compared to a small structural system with minimal external constraints. The design joist was a 20-foot 16K2 steel joist with the loading applied at the locations shown in Fig. 2. The joist was analyzed for three loading scenarios with an increasing hanging load summarized in Table 1 where LL is the design live load

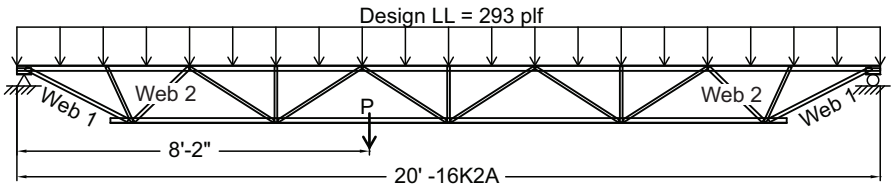

Figure 2: Overall steel joist with applied loads. Web members without a cross-section label are all Web 3.

Table 1: Test load matrix

Loading Scenario	Uniform Load	Maximum Hanging Load
LS 1	0.5 LL	100 lb
LS 2	1.0 LL	100 lb
LS 3	0 LL	280 lb

from SJI's standard joist load tables (SJI, 2020). The joist was fabricated with cold-formed steel sections with the profile shown in Fig. 3. The top and bottom chords were double equal leg angles with the nominal dimensions provided in Table 2 and a 1-1/8 inch gap between the angles. The webs were three different rolled channels with dimensions also in Table 2. The majority of the web members were cross-section Web 3 with the first two web diagonals from each end Web 1 and Web 2, respectively, as labeled in Fig. 2. Diagonal cross bracing at both ends of the joist provided lateral support to the bottom chord while the top chord was assumed to be continually braced by metal decking. This baseline information was used to create the experimental set-up and computational models.

3. Experimental Setup

Testing was performed on a two joist configuration as shown in Fig. 4 in the Jun and Sandy Lee Wisconsin Structures and Materials Testing Laboratory at the University of Wisconsin-Madison. Two 20-foot 16K2 steel joists were placed 4 feet on center with diagonal cross bracing at each end of the joists. A 6-foot wide section of metal decking was attached to the top chords of each joist with #12 Teks 5 self-drilling screws in a 36/4 pattern alternating top chord members with 2 additional sidelap fasteners. The two joists with decking and bracing provided a self-stabilizing system where external lateral support was not required during the application of the test loads.

Uniform gravity load was simulated using barrels of aggregate distributed along the length and width of the deck. The target 297 plf design live load was achieved with a total of 6077 lbs in 8 barrels and 12173 lbs in 16 barrels being applied to the deck to obtain the desired 0.5LL and

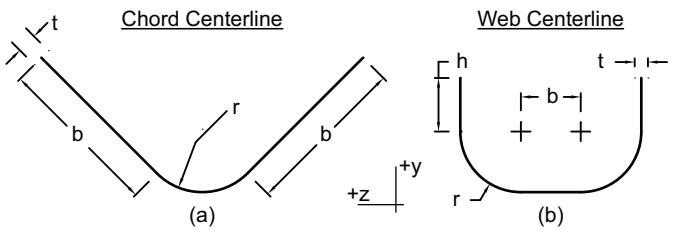

Figure 3: Typical cross-section centerlines

Table 2: Joist element cross-section centerline dimensions in accordance with Fig. 3

Section	b (in)	h (in)	r (in)	t (in)
Top Chord	1.0535	-	0.3795	0.1340
Bottom Chord	1.0100	-	0.3700	0.1150
Web 1	0.2700	0.5844	0.3700	0.1150
Web 2	0.2900	0.5258	0.3650	0.1050
Web 3	0.3466	0.3102	0.3509	0.0767

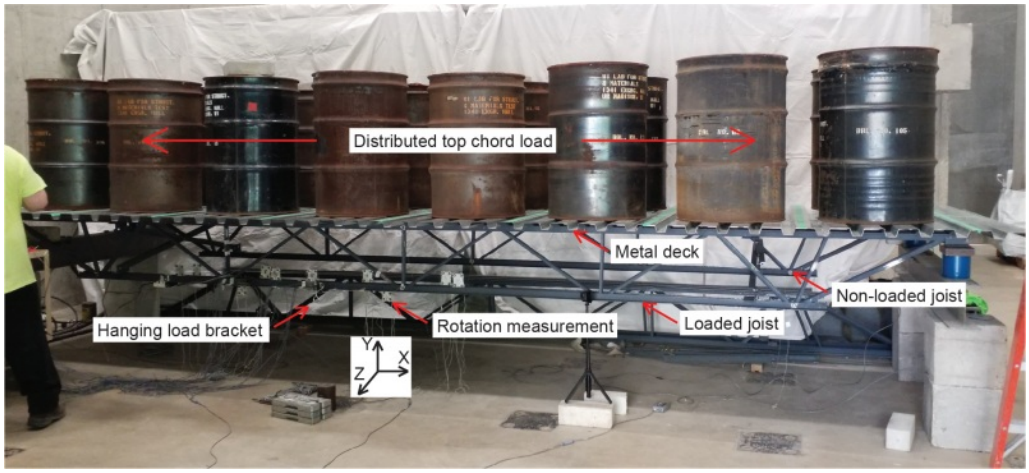

Figure 4: Experimental joist configuration

1.0LL, respectively. This applied loading corresponded with a linear load of 152 plf and 304 plf. The hanging load was applied through a 3/8" rod beam clamp attached to the bottom chord as shown in Fig. 5 causing an eccentric loading condition similar to Fig. 1(b). The 3/8" eye-bolt supported a hanging apparatus that was loaded incrementally after the appropriate uniform live load was applied.

Deflections and strain gauge measurements were recorded during each loading scenario using the self-weight of the system as the zero condition. Displacements were captured using the Optotrak system. The Optotrak system utilizes three optical sensors to track the position of markers that are attached to the structure with up to an accuracy of 0.004 in. The translation of the bottom chord was recorded at the applied load and at midspan on both joists. Rotations were obtained along the bottom chord members of the eccentrically loaded joist. The rotations were calculated based on the displacements of a group of 4 markers attached to the vertical leg of the chord as shown in Fig. 5. The rotations were recorded at the 10 locations shown in Fig. 6. Also included are the 5 positions where strain gauge measurements were taken, 2 locations on the web and 3 locations on the bottom chord. Position W1 was located at the top of vertical web to the left of the applied load. Position W2 was located at the bottom of web member directly above the applied load. Position A1 was located near the web intersection to the left of the applied load on the angle where the load was applied. Position A2 and A3 were both located at midspan but on the loaded and non-loaded angle, respectively. At each location, four linear strain measurements were recorded to allow for the calculation of the internal stresses including for the possibility of a non-zero bimoment in addition to a torsional strain measurement. The strain information was used to calculate internal

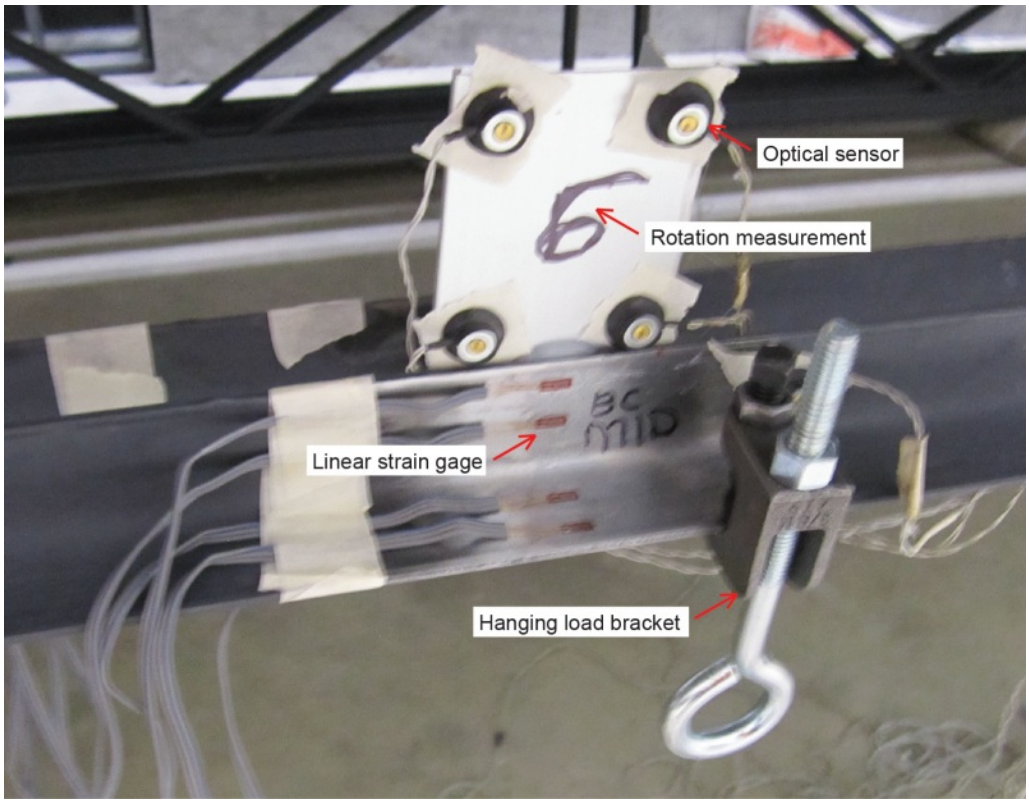

Figure 5: Hanging load application

forces based on the assumption of a linear elastic response according to the relationship shown in Eq. 1:

$$\sigma = \frac{P}{A} - \frac{M_y z}{I_y} - \frac{M_z y}{I_z} + \frac{B\omega}{C_w} \tag{1}$$

where σ is the normal stress at a position (y, z) on the cross section, P is the axial force, M_y and M_z are the bending moments about the y- and z-axes respectively, B is the bimoment, A is the area, I_y and I_z are the area moments of inertia about the y- and z-axes respectively, ω is the normalized warping coordinate, and C_w is the warping constant. This calculation of stress was completed in the local principal orientation.

4. Computational Model

The joist model created in MASTAN2 was defined to align with common design engineering practices considering SJI's recommendations for the evaluation of existing joists (Fisher and Green, 2007). It was assumed that no joint eccentricity was required to be considered at the webs resulting in the geometry shown in Fig. 7. The web members were assumed to be pinned in plane to match the typical design approach, but the webs were fixed for bending out-of-plane and warping at the ends to resist the out-of-plane moments from the eccentric loading. While not done in typical joist models for in-plane loads, the individual angles in the top and bottom chords were modeled as separate elements to allow for the independent response of the angles. At the intersection of

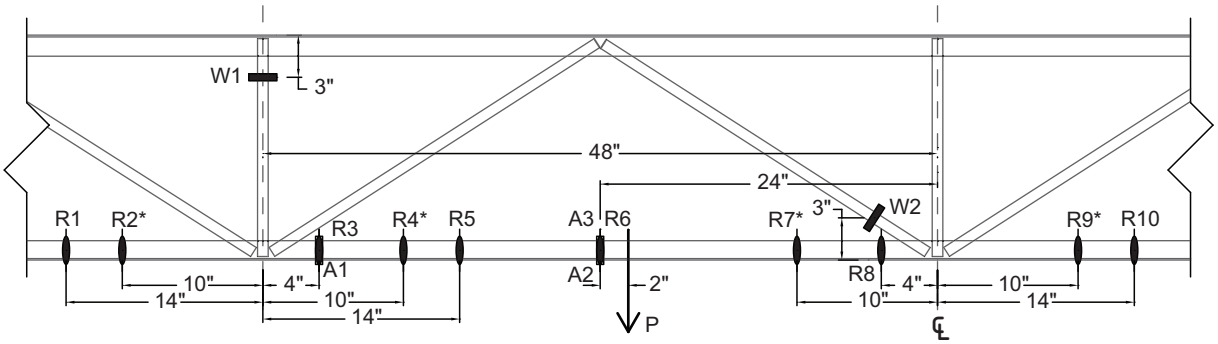

Figure 6: Locations where data was recorded on the bottom chord. Rotation information positions are marked with R where * indicates the values are for non-loaded chord instead of the loaded chord. Strain measurement locations for the two channel webs, W1 and W2, and three on the bottom chords. A1 and A2 were taken on the loaded angle while A3 was on the unloaded angle at the same position along the length as A2.

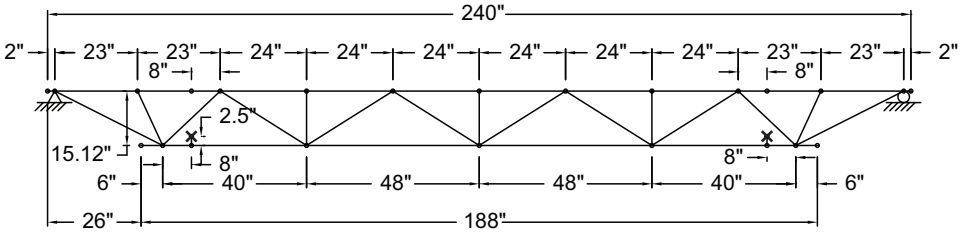

Figure 7: Joist model critical dimensions in plan

webs and chords, fixed-end rigid links with warping released were used to connect the various members. Boundary conditions were applied at the centerline of the joist using the middle node of the appropriate rigid connections. The bearing supports of the joist were treated as a pin and roller combination. A lateral support was applied to the top chord at all chord-to-web connections to approximate the deck restraint. The bottom chord was restrained with a lateral support at each end, noted by the 'X' in Fig. 7, which simulated the eccentric position of the cross bracing connection using rigid links. The cross-section properties were determined using the MSASect tool within MASTAN2 based on the centerline model of each cross section shown in Fig. 3 in a principal orientation. The modulus of elasticity was taken as 29,000 ksi with a Poisson's ratio of 0.3 for all steel elements (SJI, 2020).

The members in the MASTAN2 model were defined with continuous warping along each element resulting in consideration of bimoment. The element mesh was refined more in areas where twist was of interest until a minimal change in the maximum value of the bimoment was observed. The top chord was meshed into 4 inch segments. The webs were divided into 12 elements resulting in 1.3 to 2.4 inch long segments. The bottom chord was predominately meshed into 2 inch segments. The bottom chord bay where the hanging load was located was further refined into 0.5 inch segments within 2 inches of the applied load and 1 inch segments for the rest of that bay plus 4 inches beyond the web intersection.

The loading of the MASTAN2 model was defined to match with the magnitude applied during the

Table 3: Vertical deflection at midspan of joists before hanging load applied

Loading Scenario	Test Joist	Support Joist	First-Order	Second-Order
LS 1 w/ 0 lb	-0.361 in	-0.403 in	-0.299 in	-0.300 in
LS 2 w/ 0 lb	-0.721 in	-0.777 in	-0.600 in	-0.601 in

experimental portion of the project. Utilizing the applied load from the barrels, uniform loads of 6.33 lbs per inch and 12.68 lbs per inch were applied equally to the two top chord angles. The eccentric load was applied at the bottom of the eye bolt. The bracket was modeled with a 1.5 inch horizontal rigid link that supported a 2.5 inch, 3/8" round vertical steel section representing the eye bolt shaft. The system was analyzed using both a first-order elastic analysis and second-order elastic analysis. For the second-order analysis, the models were first solved for the uniform loading condition alone and then the hanging loads were added to the analysis to match the experimental condition.

5. Results

In comparing the physical experiments to the MASTAN2 analyses, the primary results of interest where the internal stress distributions and deformations of the bottom chords. Stresses were considered of greater importance than internal forces as the evaluation of members subjected to torsion is not covered by the current SJI Specification (2020) and the applicable section of the Specification for Structural Steel Buildings (AISC, 2016) is based on stress limit state checks. The deformation information allowed for an overall verification of the main structural behavior of the system. The physical experiments were observed to have approximately 20% greater vertical deflections in the test joist compared to the analysis models as summarized in Table 3 with minimal lateral deflections. Despite this initial variation, it was observed that the net displacements near the applied load during the experiment were similar as shown in Fig. 8. In the absence of the applied uniform load, the results presented greater agreement as illustrated in Fig. 9.

Even with the larger variation in the initial deflections, the initial axial forces in the joist bottom chords were found to have less than a 2.5% difference between the experiment and the MASTAN2 models as presented in Table 4. As such, it was determined that it was appropriate to compare the different stress distributions using the full magnitude of the internal stresses using Eq. 1 as well as the net change in stress due to the hanging load. The general distribution of stresses was found to have similarities between the bottom chord in the experiment and the MASTAN2 evaluation. The internal stresses were observed to be primarily in tension with similar distributions during Loading Scenarios 1 and 2 as shown in Fig. 10 and Fig. 11 for position A1, in Fig. 12 for position A2, and in Fig. 13 for position A3. The variations between these diagrams are highlighted when looking at the net stress diagrams in Fig. 14, Fig. 15, and Fig. 16. The largest variation in the stress distributions was associated with position A2 near the applied load where the net compression effects from biaxial bending moments on the vertical leg of the bottom chord was greater in the computational models than the experimental results. Loading Scenario 3 results were used to produce the stress distributions in Fig. 17, Fig. 18, Fig. 19, and Fig. 20 which isolated the ability of the computational analysis to account for the appropriate effects of the eccentric loading. These results from Loading Scenario 3 present similar stress distributions as observed when looking at the net stresses from Loading Scenarios 1 and 2, but with better agreement between the experimental

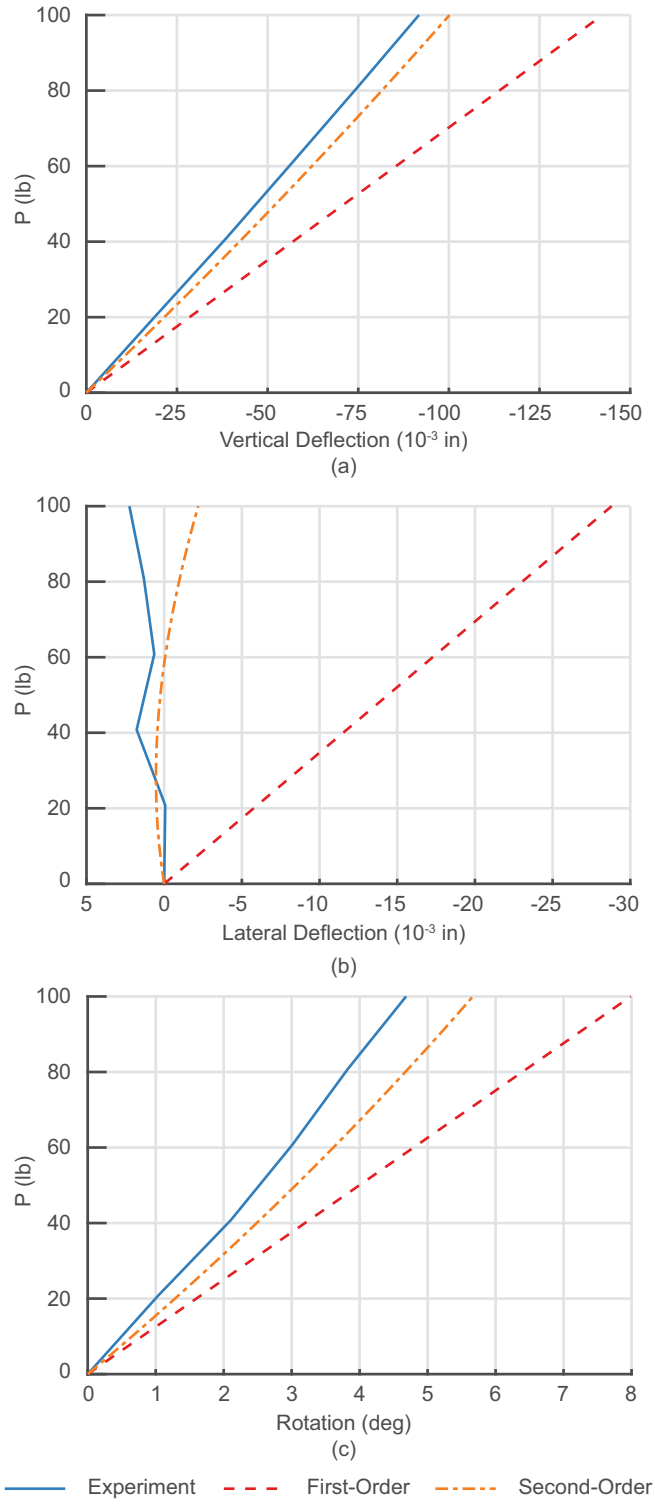

Figure 8: Net displacement of bottom chord at the hanging load in Load Scenario 2 in the global orientation shown in Fig. 4. (a) Vertical deflection in the Y-direction (b) Lateral displacement in the Z-direction (c) Torsional rotation about the X-axis

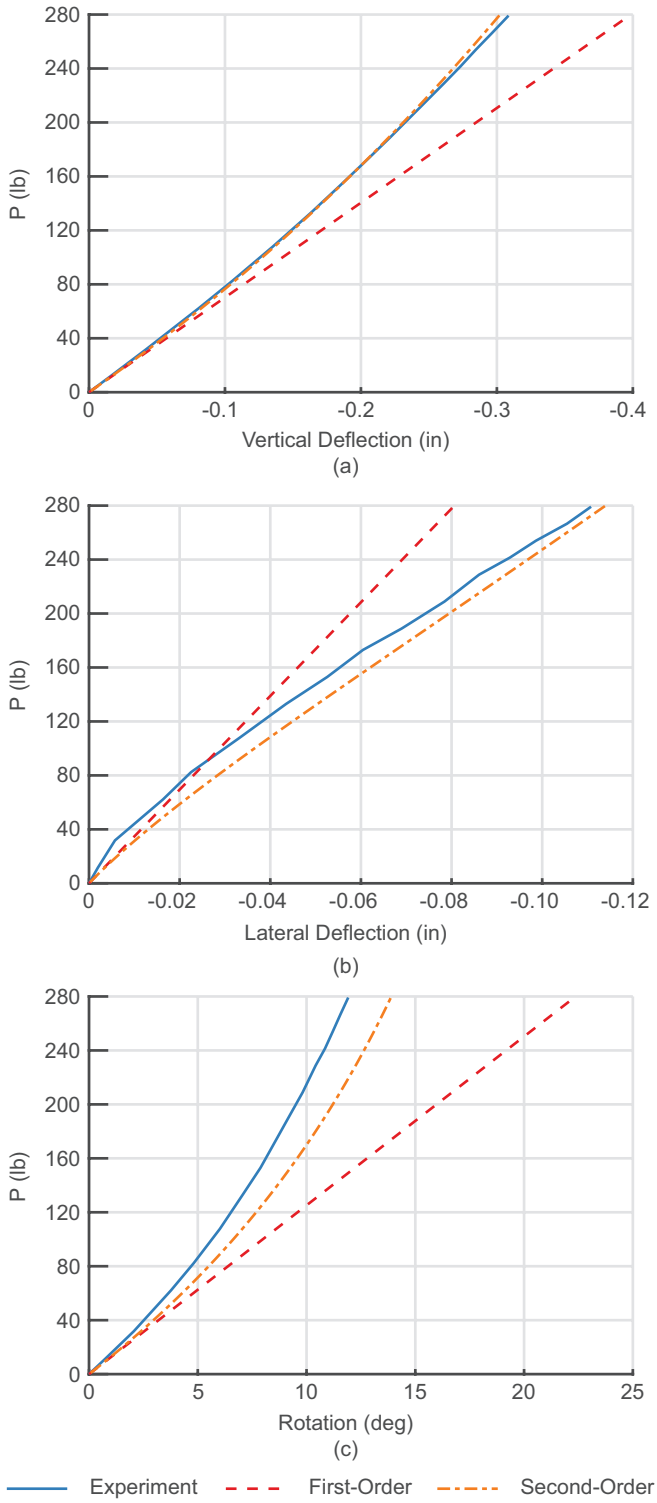

Figure 9: Displacement of bottom chord at the hanging load in Load Scenario 3 in the global orientation shown in Fig. 4. (a) Vertical deflection in the Y-direction (b) Lateral displacement in the Z-direction (c) Torsional rotation about the X-axis

Table 4: Axial force in bottom chord before hanging load applied

Loading Scenario	Experiment at A2	Experiment at A3	First-Order	Second-Order
LS 1 w/ 0 lb	2781 lb	2801 lb	2800 lb[1]	2802 lb[1]
LS 2 w/ 0 lb	5741 lb	5741 lb	5609 lb[1]	5617 lb[1]

[1] The force is the same in both chords in the analysis model prior to the application of the hanging load.

Table 5: Maximum tensile stress in bottom chord

		Stress [ksi] (Error to Experiment)		
Position	Loading Scenario	Experiment	First-Order	Second-Order
A1	LS 1 w/ 0 lb	10.96	9.86 (-10.1%)	9.96 (-9.2%)
	LS 1 w/ 60 lb	10.93	12.59 (15.2%)	11.46 (4.8%)
	LS 1 w/ 100 lb	12.86	15.24 (18.5%)	13.73 (6.8%)
	LS 2 w/ 0 lb	22.34	19.75 (-11.6%)	20.08 (-10.1%)
	LS 2 w/ 60 lb	21.79	22.47 (3.1%)	20.34 (-6.6%)
	LS 2 w/ 100 lb	21.61	24.29 (12.4%)	20.95 (-3.1%)
A2	LS 1 w/ 0 lb	10.16	9.90 (-2.6%)	9.97 (-1.9%)
	LS 1 w/ 60 lb	14.31	14.50 (1.4%)	13.08 (-8.6%)
	LS 1 w/ 100 lb	16.81	17.62 (4.8%)	15.01 (-10.7%)
	LS 2 w/ 0 lb	20.44	19.82 (-3.0%)	20.00 (-2.2%)
	LS 2 w/ 60 lb	24.06	24.37 (1.3%)	22.23 (-7.6%)
	LS 2 w/ 10 lb	26.30	27.48 (4.5%)	23.88 (-9.2%)
A3	LS 1 w/ 0 lb	11.14	9.90 (-11.2%)	9.97 (-10.6%)
	LS 1 w/ 60 lb	11.81	10.98 (-7.0%)	10.79 (-8.7%)
	LS 1 w/ 100 lb	12.19	11.70 (-4.0%)	11.30 (-7.3%)
	LS 2 w/ 0 lb	22.76	19.82 (-12.9%)	20.01 (-12.1%)
	LS 2 w/ 60 lb	23.42	20.90 (-10.7%)	20.68 (-11.7%)
	LS 2 w/ 100 lb	23.85	21.63 (-9.3%)	21.11 (-11.5%)

results and MASTAN2, similar to the displacement results shown earlier.

While different values would also be of interest, a significant stress value from Load Scenario 1 and 2 that would be used in design would be the maximum tensile stress found in the section. Due to differences prior to the application of the hanging load, the maximum stresses observed in the chord from the MASTAN2 results were commonly found to be less than the experimental values as shown in Table 5. However, Table 6, which compares only the change to the maximum tensile stress on the cross section from the hanging load, summarized that the results for MASTAN2 were determined to be conservative at position A1 and A3 but unconservative at A2. The stress distribution at most positions on the cross section were conservative for the effect of the bending moments added to the structure, but this meant that a conservative value of compression was added to the vertical leg of the bottom chord which reduced the maximum tension. This is reinforced looking at the maximum tensile and compressive stresses from Loading Scenario 3 in Table 7 where the MASTAN2 results are conservative except for the tension effects in the horizontal leg at A2.

While data was recorded for the stresses in the webs, no values are presented in this paper. The values were recorded near the ends in an attempt to verify the fixity of the connection of the web members to the chords in the out-of-plane orientation. The resulting experimental data did not

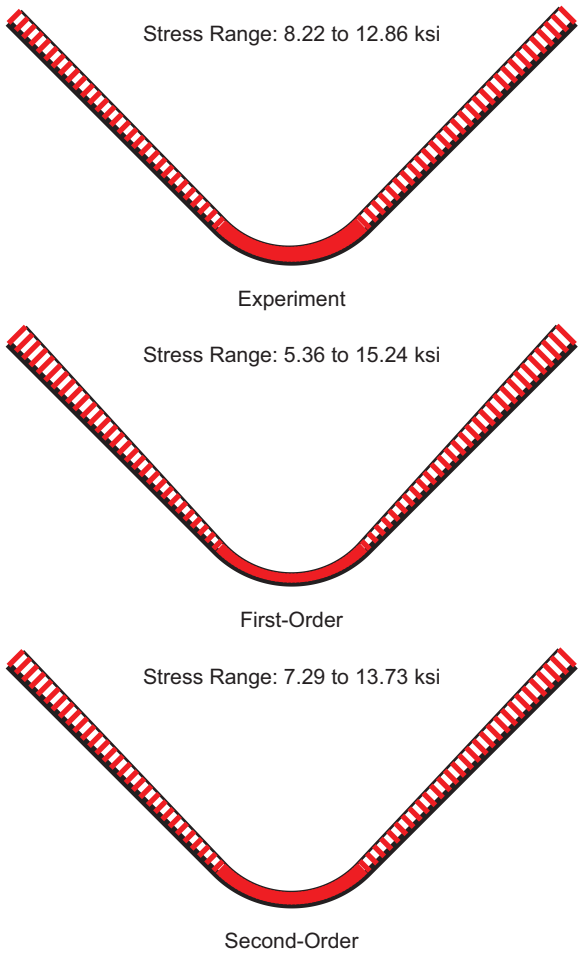

Figure 10: Normal stresses on bottom chord at A1 for Loading Scenario 1 with 100 lb hanging load

Table 6: Maximum change in tensile stress in bottom chord based on net effect

		Stress [ksi] (Error to Experiment)		
Position	Loading Scenario	Experiment	First-Order	Second-Order
A1	LS 1 w/ 60 lb	2.92	4.34 (48.8%)	3.61 (23.7%)
	LS 1 w/ 100 lb	4.85	7.24 (49.4%)	5.88 (21.4%)
	LS 2 w/ 60 lb	2.59	4.34 (67.5%)	3.29 (26.8%)
	LS 2 w/ 100 lb	4.36	7.24 (65.9%)	5.36 (22.9%)
A2	LS 1 w/ 60 lb	4.15	4.68 (12.9%)	3.36 (-19.0%)
	LS 1 w/ 100 lb	6.65	7.80 (17.2%)	5.28 (-20.7%)
	LS 2 w/ 60 lb	3.62	4.68 (29.1%)	2.85 (-21.3%)
	LS 2 w/ 100 lb	5.86	7.80 (33.0%)	4.49 (-23.4%)
A3	LS 1 w/ 60 lb	0.67	1.08 (63.1%)	0.82 (22.8%)
	LS 1 w/ 100 lb	1.05	1.81 (72.4%)	1.34 (27.4%)
	LS 2 w/ 60 lb	0.66	1.08 (64.7%)	0.67 (2.5%)
	LS 2 w/ 100 lb	1.09	1.81 (65.6%)	1.11 (1.3%)

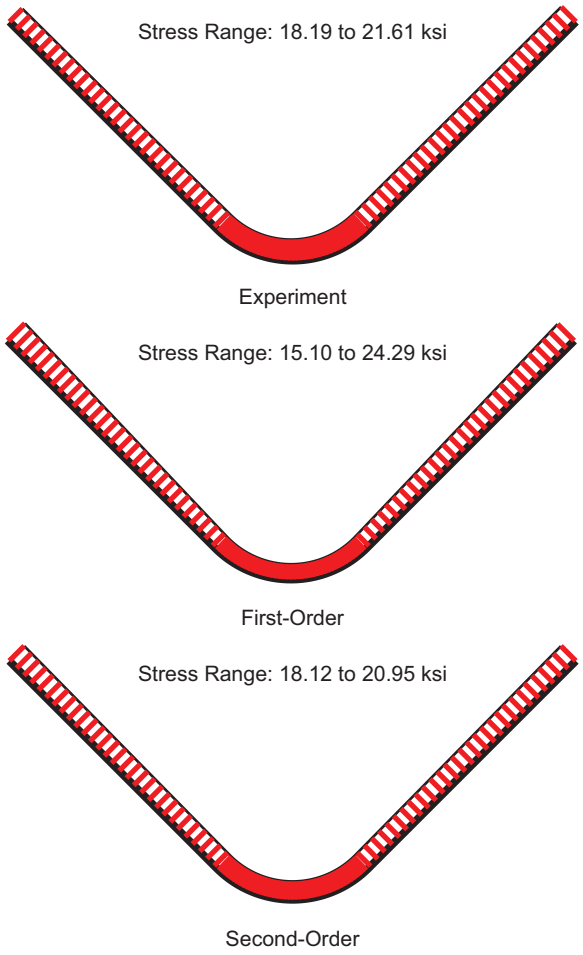

Figure 11: Normal stresses on bottom chord at A1 for Loading Scenario 2 with 100 lb hanging load

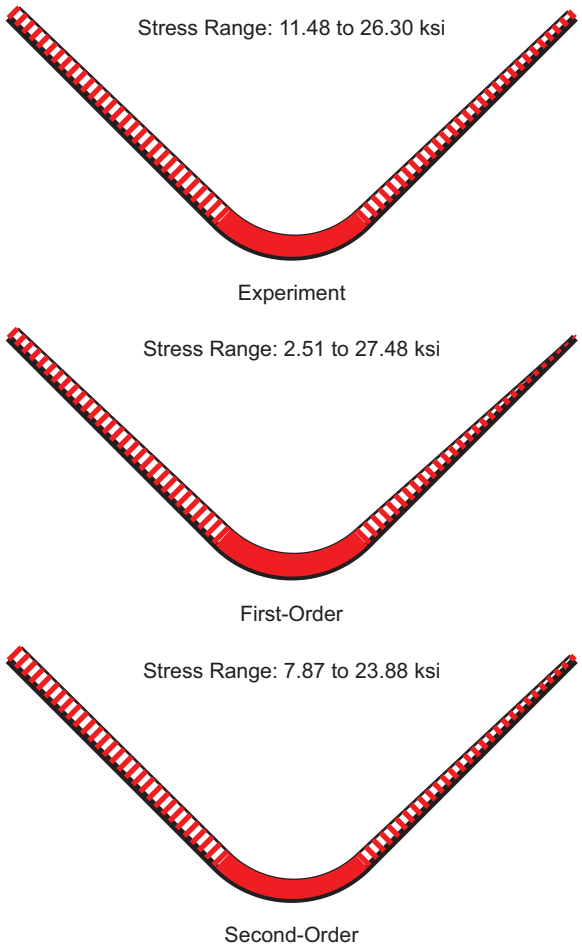

Figure 12: Normal stresses on bottom chord at A2 for Loading Scenario 2 with 100 lb hanging load

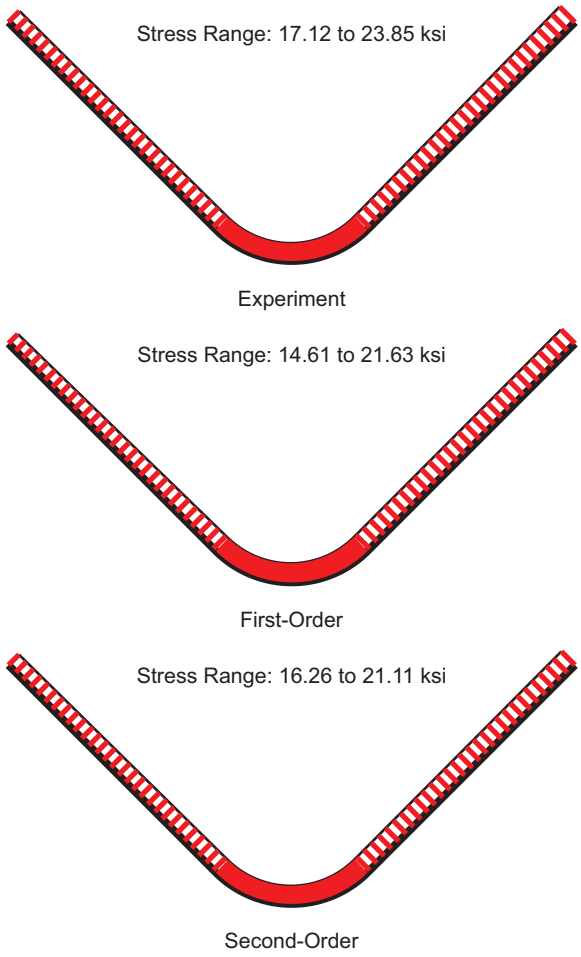

Figure 13: Normal stresses on bottom chord at A3 for Loading Scenario 2 with 100 lb hanging load

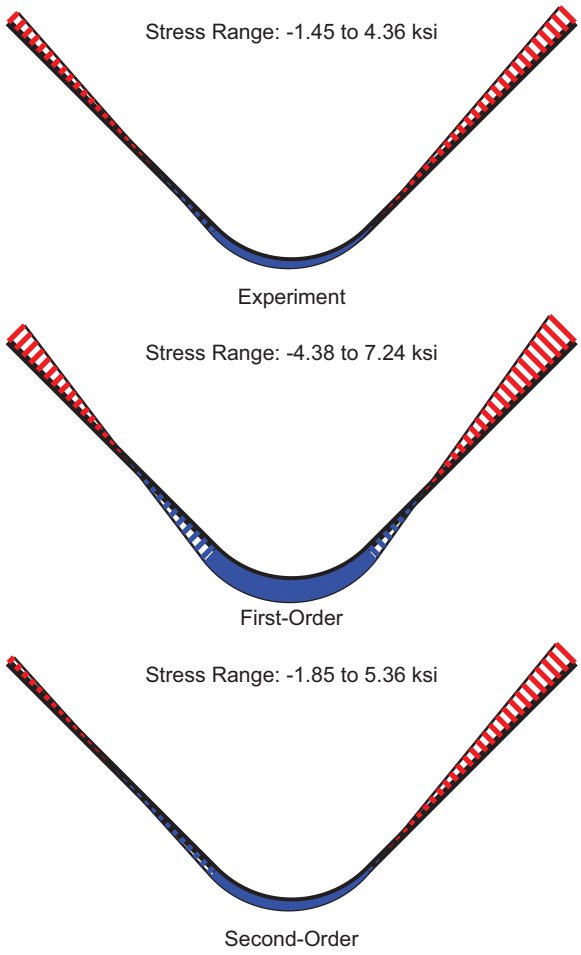

Figure 14: Net normal stresses on bottom chord at A1 for Loading Scenario 2 with 100 lb hanging load

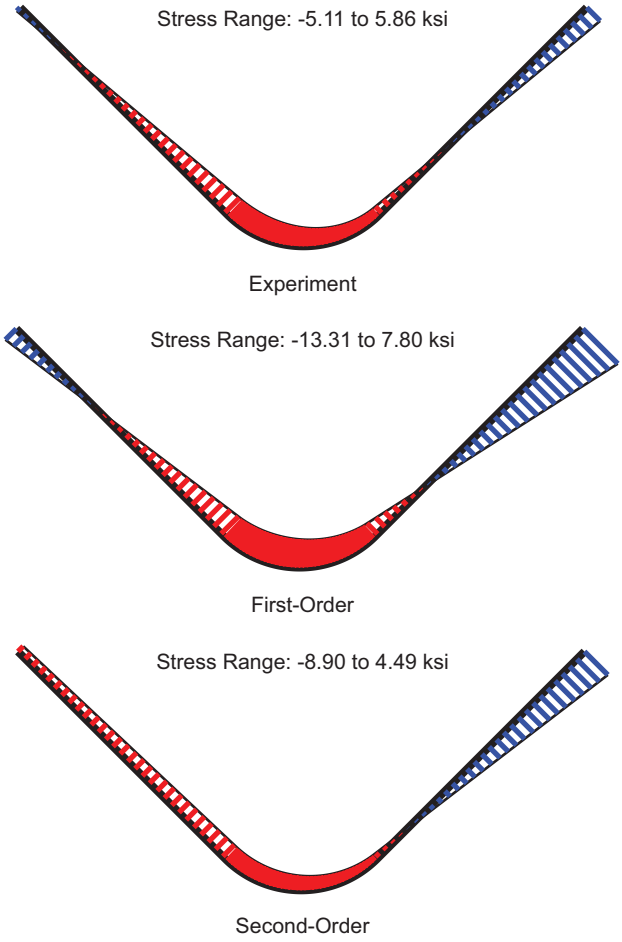

Figure 15: Net normal stresses on bottom chord at A2 for Loading Scenario 2 with 100 lb hanging load

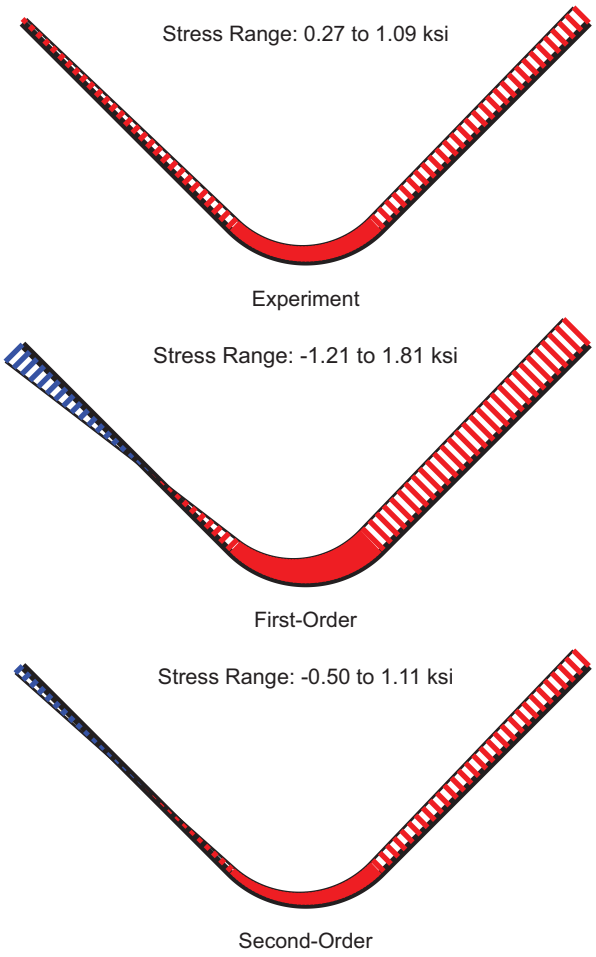

Figure 16: Net normal stresses on bottom chord at A3 for Loading Scenario 2 with 100 lb hanging load

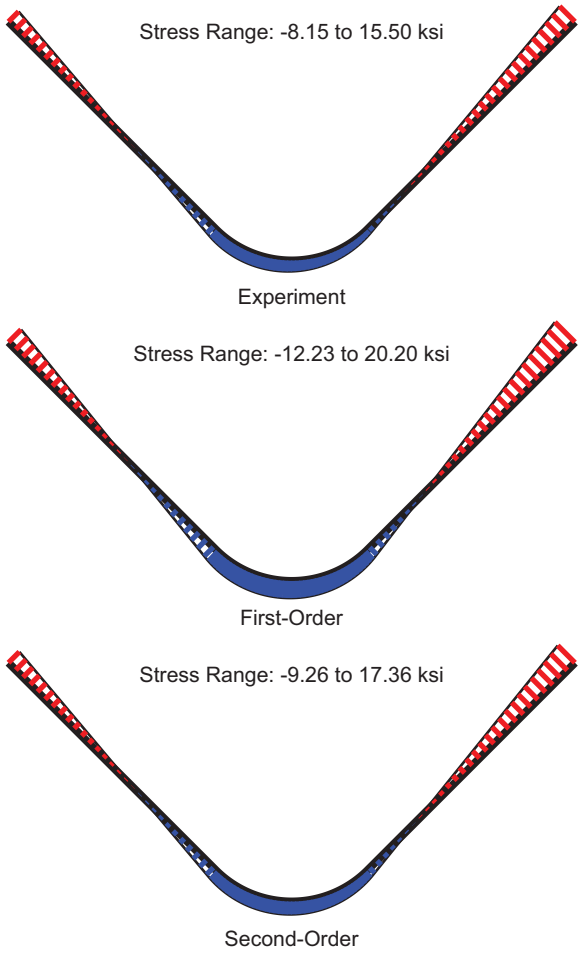

Figure 17: Normal stresses on bottom chord at A1 for Loading Scenario 3 with 279 lb hanging load

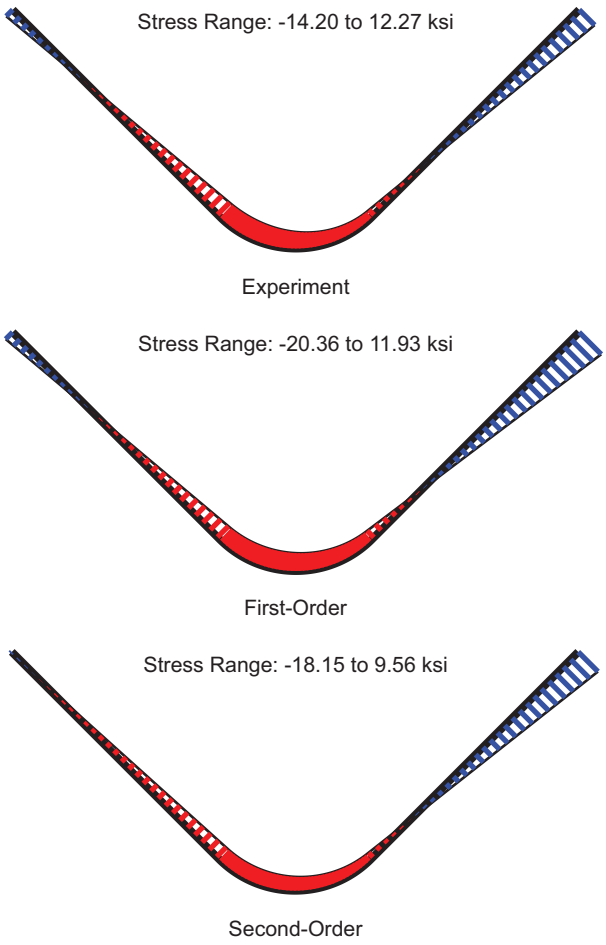

Figure 18: Normal stresses on bottom chord at A2 for Loading Scenario 3 with 153 lb hanging load

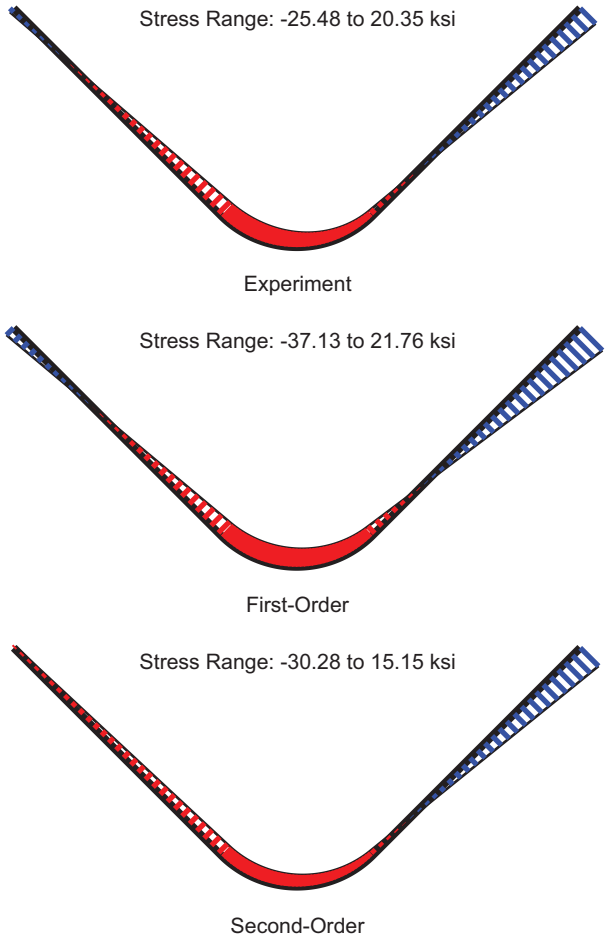

Figure 19: Normal stresses on bottom chord at A2 for Loading Scenario 3 with 279 lb hanging load

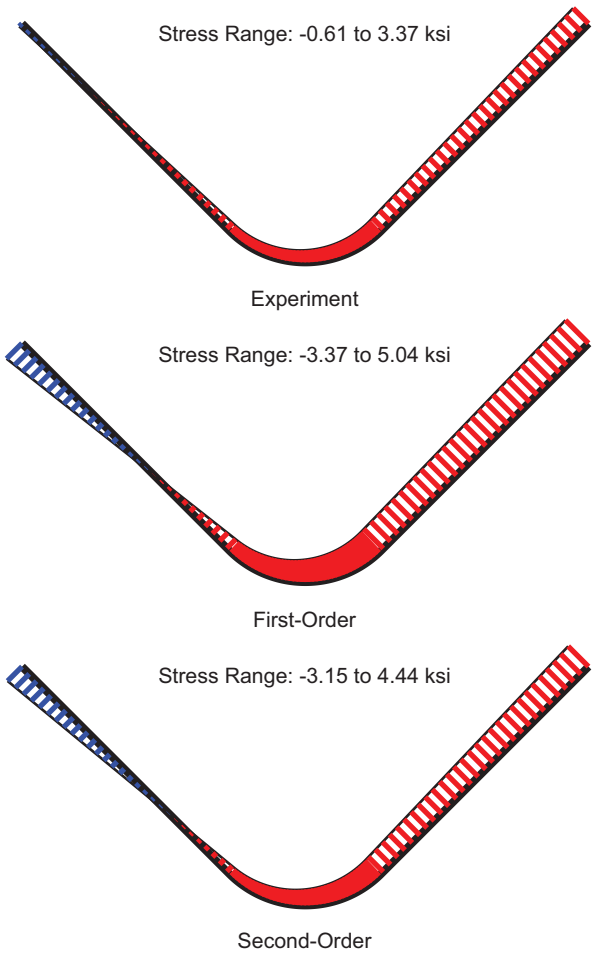

Figure 20: Normal stresses on bottom chord at A3 for Loading Scenario 3 with 279 lb hanging load

Table 7: Extreme stresses in bottom chord for Loading Scenario 3

Position	Hanging load		Stress [ksi] (Error to Experiment)		
			Experiment	First-Order	Second-Order
A1	82 lb	Max	4.94	5.94 (20.0%)	5.63 (13.9%)
		Min	-2.77	-3.59 (29.8%)	-3.30 (19.1%)
	153 lb	Max	8.92	11.08 (24.2%)	10.09 (13.2%)
		Min	-4.93	-6.70 (36.0%)	-5.72 (16.0%)
	209 lb	Max	11.89	15.13 (27.2%)	13.41 (12.7%)
		Min	-6.43	-9.16 (42.4%)	-7.40 (15.0%)
	279 lb	Max	15.50	20.20 (30.3%)	17.36 (12.0%)
		Min	-8.15	-12.23 (49.9%)	-9.26 (13.5%)
A2	82 lb	Max	7.07	6.39 (-9.5%)	5.64 (-20.1%)
		Min	-7.66	-10.91 (42.4%)	-10.27 (34.0%)
	153 lb	Max	12.27	11.93 (-2.7%)	9.56 (-22.0%)
		Min	-14.20	-20.36 (43.4%)	-18.15 (27.8%)
	209 lb	Max	16.03	16.30 (1.6%)	12.22 (-23.8%)
		Min	-19.26	-27.82 (44.4%)	-23.80 (23.6%)
	279 lb	Max	20.35	21.76 (6.9%)	15.15 (-25.5%)
		Min	-25.48	-37.13 (45.7%)	-30.28 (18.9%)
A3	82 lb	Max	1.10	1.48 (35.1%)	1.43 (30.6%)
		Min	-0.19	-0.99 (432.0%)	-0.96 (417.2%)
	153 lb	Max	1.95	2.77 (41.6%)	2.59 (32.3%)
		Min	-0.36	-1.85 (416.8%)	-1.77 (393.6%)
	209 lb	Max	2.58	3.78 (46.4%)	3.44 (33.3%)
		Min	-0.47	-2.53 (437.6%)	-2.39 (407.8%)
	279 lb	Max	3.37	5.04 (49.8%)	4.44 (32.0%)
		Min	-0.61	-3.37 (450.7%)	-3.15 (414.5%)

correspond to the assumption of a stress distribution defined by Eq. 1. The stresses were indicative of a stress concentration still occuring due to the proximity of the welded connection. At the bottom of the web at location W2, the leg of the channel attached to the chord angle with the hanging load applied had a significantly larger stress. Location W1 at the top of a web presented a better distribution of force to both sides of the channel, but the large difference between the measurements near the tip of the channel versus closer to the flat bottom implied that significant bimoment and bending in both directions would need to exist for the distribution to align with Eq. 1. In both cases, the measured results was something that MASTAN2 would not be expected to reproduce and as such excluded from this paper.

6. Discussion

The evaluations of the joist model in MASTAN2 provided a good prediction of the internal stresses in the bottom chord. The first-order results were consistently larger than the second-order results and did correspond with better agreement with the total stresses presented from Loading Scenario 1 and 2. However, this agreement seems to be largely an artifact of the initial underestimating of the internal stresses due to the distributed load by both methods combined with an overestimating of the effects of the hanging load in the first-order analysis. As was presented in Table 7, the calculated changes due to the first-order analysis are significantly larger than the measured response. The second-order analysis provided better agreement with the experimental data. This larger variation was attributed primarily to the factor that the second-order analysis evaluated the forces on the rotated section and included the deformation of the hanger bracket. Due to the rotation of the angle chord and bracket plus the bending of the hanger rod, the distance from the applied load to the angle shear center was reduced. This movement reduced the torsional loading in the second-order analysis and decreased the overall twist of the section. With this updated orientation, the second-order analysis solution included less bending moment in the weak-axis of the chord and more strong-axis bending compared to the first-order analysis for the same global moment changing the stress distribution.

The displacement information recorded allowed for determination of the twist of both bottom chords separately. As was shown in Fig. 8 and Fig. 9, the second-order analysis in MASTAN2 was able to predict rotation behavior of the loaded chord better than the first-order analysis. In both cases, the MASTAN2 result was larger than the actual experiment, but displayed the correct behavior. The rotation of the non-loaded chord angle in Fig. 21(a) similarly indicated agreement between the analysis methods and the experiment result away from the eccentric load. However, in the bay where the load was applied the non-loaded chord was observed to exhibit limited rotation during the experiment, Fig. 21(b). In the presence of the axial force from Loading Scenario 1 and 2, the non-loaded chord similarly exhibited smaller rotations than would be expected from the computation result. Combining this reduced twist with the stress concentrations observed in one side of the web channel at W2, there are likely effects of the web channels deforming in the plane of the cross section that is contributing to the discrepancy between the experimental and computational results from this uneven loading. While this response cannot be differently modeled with the elements considered, future investigation into an appropriate stiffness of the chord to web connection could possibly improve the bending moment representation in each chord. The current rigid link connection is causing a bending and twisting response that is similar to a fixed-fixed

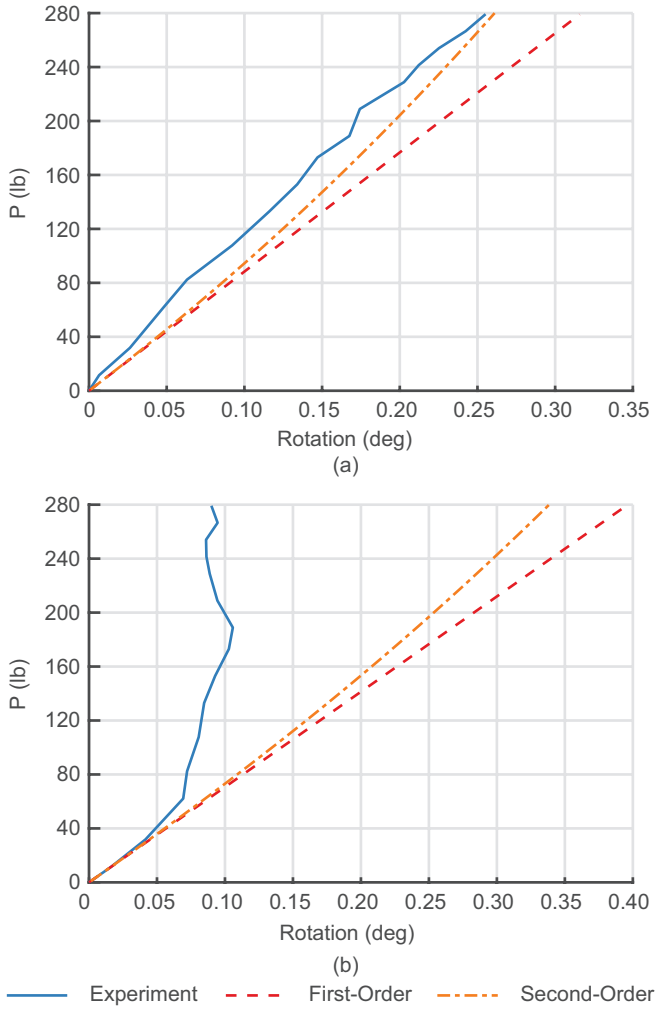

Figure 21: Rotation of non-loaded bottom chord for Loading Scenario 3. (a) In bay to the left of applied load and (b) In same bay as applied load

boundary condition.

7. Ongoing Work: Section Imperfection

In the process of in this project it was observed that the cold-formed members, particularly the web channel cross sections, exhibited visible variations from the nominal geometry. As a result, the web members nearest the strain gauges were measured using the Artec Leo, a handheld 3D scanner, utilizing the methodology discussed by Xia and Blum (2020). Following the completion of the experiment, the joist under consideration was scanned to obtain the necessary point cloud information to determine the web cross section. The joist was scanned while in four different orientations to obtain overlapping point cloud data to be able to reconstruct a section of the joist in the Artec Studios software (Artec 3D, 2018). After creating a fusion model of the data, the information was imported into MATLAB (MathWorks, 2019). The point cloud data was then subdivided into the different structural components. The separate components could then be segmented along the length to determine the cross section for a slice of the structure at any location as shown in

Table 8: Measured versus nominal web section properties

Section Property	Nominal	Measured	Difference
A (in^2)	0.159	0.157	-1.3%
J (in^4)	3.11 x 10^{-4}	3.07 x 10^{-4}	-1.3%
I_z (in^4)	7.27 x 10^{-3}	7.89 x 10^{-3}	8.6%
I_y (in^4)	2.76 x 10^{-2}	2.65 x 10^{-2}	-4.0%
Shear center y coordinate (in)	-0.472	-0.489	3.7%
Shear center z coordinate (in)	0.000	0.002	N/A
C_w (in^6)	7.62 x 10^{-4}	3.87 x 10^{-4}	-49.2%

Fig. 22(a). The point cloud data was used to create a curve that defined the exterior profile of the web. This curve was offset based on the nominal thickness of the member to define the approximate center line profile of the scan information. The exterior portion of the center line curve was extracted and then extended based on the exterior profile to define the complete center line profile shown in Fig. 22(b).

As depicted in Fig. 23, the measured cross section for Web 3 did not exhibit the sharp 90° bends associated with the nominal cross section. This alternation to the cross section resulted in significant changes to the section properties shown in Table 8, particularly the moment of inertia about the z-axis and the warping constant. For the work presented, this altered geometry was primarily used with the experimentally measured web strains in an attempt to improve the calculated stress profile. As previously mentioned, it was determined the web measurements captured localized connect effects which could not be represented by the analyses considered and as a result this line of investigation was paused. The effect of considering the measured geometry compared to the nominal geometry of the various cross sections in the overall analysis is ongoing.

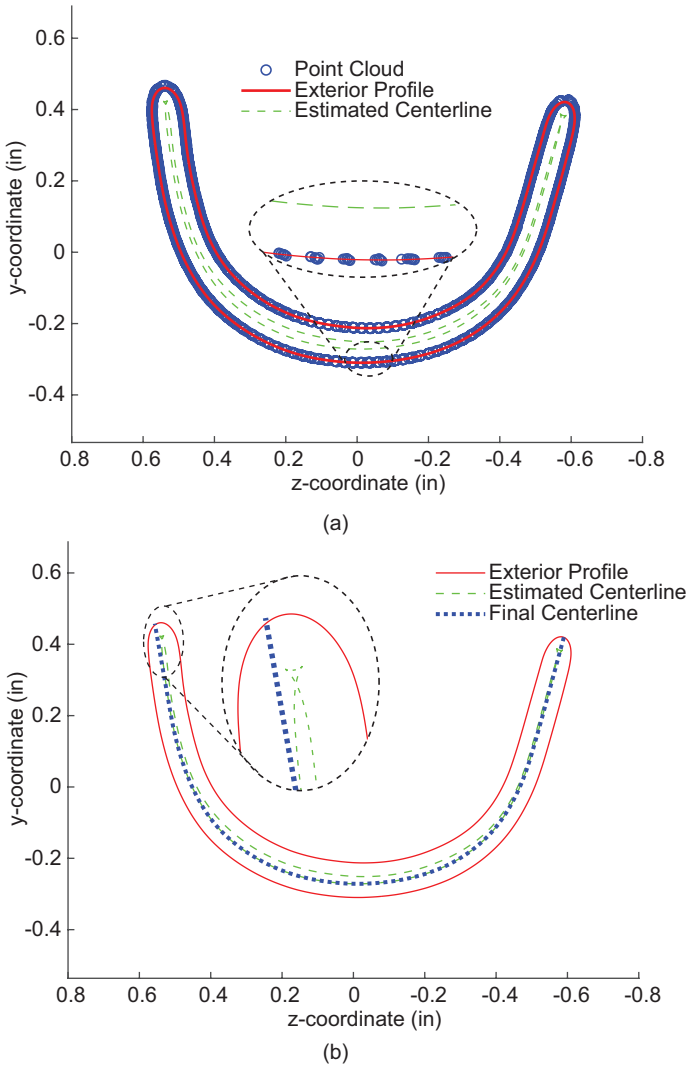

Figure 22: Point cloud data outline with representative curves. (a) Point cloud data with exterior profile. (b) Exterior profile and resulting center line information.

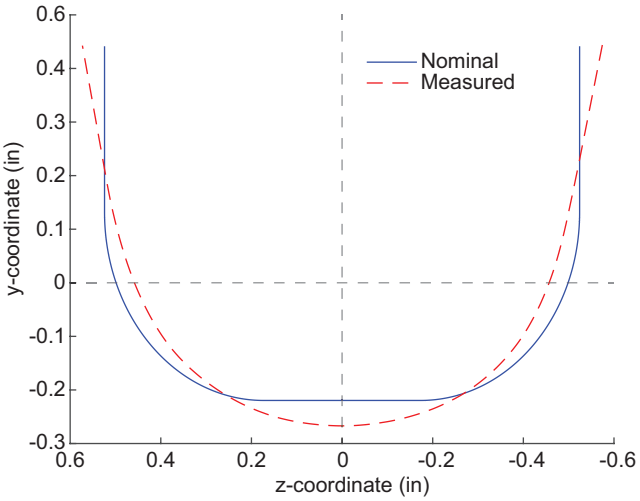

Figure 23: Measured versus nominal cross-section geometry

8. Conclusions

This paper presents the testing and evaluation of a steel joist structural assembly subjected to eccentric loading. A pair of steel joists were subjected to a fraction of simulated uniform design live load and then an eccentric hanging load was applied to one of the bottom chord angle members. During the experiment, strain and displacement information was recorded along the bottom chord. The application of the hanging load resulting in a lateral displacement of the bottom chord as well as a large twist in only the loaded member. The joist was analyzed in MASTAN2 using a first-order and a second-order analysis accounting for non-symmetric sections. Using the results from the computational work as well as the experimental data, the stress profile in the bottom chord was compared. It was determined that MASTAN2 was capable of determining a conservative stress profile for the effects of an eccentric hanging load. The results of the first-order analysis consistently produced higher stresses than the second-order analysis due to the considerations of equilibrium on the deformed structure.

Acknowledgements

The authors would like to thank New Millennium Building Systems, American Iron and Steel Institute, Steel Joist Institute, and Steel Deck Institute for their financial support of this project through the AISI Standards Council Small Project. The authors would also like to specifically thank Joe Pote and Scott Morton of New Millennium Building Systems for their input and assistance related to this project.

References

AISC (2016). *Specification for Structural Steel Buildings ANSI/AISC 360-16*. Chicago, IL: American Institute of Steel Construction, p. 676.

Artec 3D (2018). *Artec Studios 13*. Luxembourg.

Fisher, James M. and Perry S. Green (2007). *Steel Joist Institute Technical Digest 12: Evaluation and Modification of Open-Web Steel Joists and Joist Girders*. Tech. rep. Myrtle Beach, SC: Steel Joist Institute, p. 110.

Liu, Si-Wei, Wen-Long Gao, and Ronald D. Ziemian (2019). "Improved line-element formulations for the stability analysis of arbitrarily-shaped open-section beam-columns". In: *Thin-Walled Struct.* 144.July, p. 106290. DOI: 10.1016/j.tws.2019.106290.

Liu, Si-Wei, Ronald D. Ziemian, et al. (2018). "Bifurcation and large-deflection analyses of thin-walled beam-columns with non-symmetric open-sections". In: *Thin-Walled Struct.* 132.135, pp. 287–301. DOI: 10.1016/j.tws.2018.07.044.

MathWorks (2019). *MATLAB (R2019a)*. Natick, MA.

Murphy, R. Donald (1992). "The Features and Benefits of Steel Joists". In: *Constr. Dimens.* October, pp. 22–23.

Sippel, Edward J. and Hannah B. Blum (2020). "System analysis of nonsymmetric cold-formed steel cross sections members". In: *CFSRC Colloq.* 2020, pp. 1–8.

Sippel, Edward J., Ronald D. Ziemian, and Hannah B. Blum (2020). "Analysis of non-symmetric cross-sections relative to the provisions of AISC 360-10". In: *Proc. 2020 SSRC Annu. Stab. Conf.* Ed. by SSRC. Atlanta, GA: SSRC, pp. 1–28.

SJI (2020). *Standard Specifications: Load Tables and Weight Tables for Steel Joists and Joist Girders SJI 100-2020*. 45th Ed. Florence, SC: Steel Joist Institute, p. 232.

Xia, Yu and Hannah B. Blum (2020). "Geometric imperfection measurements of cold-formed steel members using a portable non-contact 3D laser scanner". In: *Proc. 2020 SSRC Annu. Stab. Conf.* Atlanta, GA: SSRC, pp. 1–15.

Ziemian, Ronald D., William McGuire, and Si-Wei Liu (2019). *MASTAN2 v5.1.20*.